JOURNAL OF MATERIALS SCIENCE 35 (2000) 2331–2345

# Microstructural study of two LAS-type glass-ceramics and their parent glass

L. ARNAULT, M. GERLAND, A. RIVIÈRE
*Laboratoire de Mécanique et Physique des Matériaux, UMR-CNRS 6617, ENSMA, B.P.40109, F-86961 Futuroscope Chasseneuil cedex, France*
*E-mail: arnault@lmpm.ensma.fr*

The two glass-ceramics studied here derive from the complex system $(MgO,ZnO,Li_2O)$-$Al_2O_3$-$SiO_2$ and are obtained by controlled devitrification of the same parent glass. Although they have the same chemical composition, one is a "$\beta$-quartz" (or "$\beta$-eucryptite") type while the other one is a "$\beta$-spodumene" glass-ceramic. A detailed microstructural analysis of these materials has been performed at different scales by several complementary characterization methods (SEM, TEM, DTA, XRD and FTIR). This extensive study has shown the great microstructure difference (grain distribution, grain size, nature of vitreous and crystalline phases) between these two glass-ceramics obtained from the same parent glass. 

## 1. Introduction

Glass-ceramic materials are polycrystalline solids prepared by controlled crystallization of shaped glass objects. The glass is subjected to a carefully regulated heat-treatment schedule which results in nucleation and crystallization of various crystalline phases.

Since the works of Stookey [1, 2] on controlled glass crystallization process, researches have led to new means of controlled nucleation, such as the introduction of nucleating agents in the parent glass. The crystallization process is generally well advanced but a residual glassy phase remains in which very small crystals (from 0.1 $\mu$m to 1 $\mu$m) are uniformly distributed. The glassy phase of glass-ceramic has not the same chemical composition as the parent glass since it is deficient in oxides which have participated to the formation of the various crystalline phases of the glass-ceramic. This glassy phase, although residual, considerably influences the microstructure of glass-ceramics and so their properties.

The glass-ceramic process is applicable to a wide range of compositions but the glass family derived from LAS ($Li_2O$-$Al_2O_3$-$SiO_2$) system is currently used for the industrial glass-ceramics production. Since the 60's, several studies on the crystallization and the microstructural evolution of LAS-type glasses have been performed [3, 4], including a very recent one [5]. The most frequently used nucleating agents are the $TiO_2$ and $ZrO_2$ oxides or their mixture which is more efficient according to Stewart [6]. The most currently LAS-type glass-ceramics, the "$\beta$-quartz" (or "$\beta$-eucryptite") and "$\beta$-spodumene" glass-ceramics, are characterized by very low thermal expansion and then are used in different fields such as consumer products, telescope mirror blanks, radomes for aerospace industry. These glass-ceramics are so called because the main crystalline phase developed in "$\beta$-quartz" and "$\beta$-spodumene" LAS-type glass-ceramics are $\beta$-eucryptite ($Li_2O$-$Al_2O_3$-$2SiO_2$)/$\beta$-quartz ($SiO_2$) solid solutions and $\beta$-spodumene ($Li_2O$-$Al_2O_3$-$4SiO_2$)/keatite ($SiO_2$) respectively. The $\beta$-quartz solid solution is based on the hexagonal $\beta$-quartz structure while the $\beta$-spodumene solid solution derives from the tetragonal form of silica known as keatite. These aluminosilicate crystalline phases composed of three-dimensional networks of $SiO_4$ and $AlO_4$ tetrahedra were termed "stuffed derivatives" by Buerger [7] because they may be thought of as formed from a silica structure by network replacement of $Si^{4+}$ by $Al^{3+}$, accompanied by a filling of interstitial vacancies by larger monovalent or divalent cations to achieve electrical neutrality.

A stuffed $\beta$-quartz solid solution generally occurs by heat-treating a glass of the general composition $Li_2O{\cdot}Al_2O_3{\cdot}nSiO_2$ with $n \geq 2$. However, except those which have a composition very close to the stoichiometric eucryptite $Li_2O{\cdot}Al_2O_3{\cdot}4SiO_2$, the $\beta$-quartz solid solutions (with $n > 3.5$) are metastable [8–10] and transform into keatite solid solutions at elevated temperatures [11]. A series of stable solid solutions is normally formed between $\beta$-spodumene ($Li_2O{\cdot}Al_2O_3{\cdot}4SiO_2$ or $LiAlSi_2O_6$) and keatite ($SiO_2$) with formula $Li_xAl_xSi_{1-x}O_2$ ($x \leq 0.366$) or $Li_2O{\cdot}Al_2O_3{\cdot}nSiO_2$ ($n \geq 3.5$). These solid solutions are variously called: $\beta$-spodumene/keatite solid solution, keatite solid solution or $\beta$-spodumene solid solution. So, each LAS composition with $n \geq 3.5$, treated at high temperature, leads to a $\beta$-spodumene solid solution. This crystalline aluminosilicate phase is moreover considered to be formed by recrystallization of a $\beta$-quartz solid solution rather than by direct glass crystallization.

The commercial glass-ceramics are generally more complex than the simple LAS system. In commercial

compositions, $Li_2O$ is partially substituted by MgO and ZnO in order to improve the parent glass work properties while lowing the cost of materials. A wide variety of LAS glasses containing additional components, such as MgO and ZnO, can be crystallized almost entirely in stuffed $\beta$-quartz solid solution [12–15]. The $Li^+$ ions in the stuffed $\beta$-quartz solid solution can be replaced by divalent $Mg^{2+}$ ions and to a smaller extent by $Zn^{2+}$ ions which have ionic radii of the same size order. With the exception of the stable $\beta$-eucryptite phase, all the stuffed $\beta$-quartz solid solutions are not stable at high temperatures and, if heated for a sufficient time at subsolidus temperatures, will transform to stable crystalline products which depend on the initial composition (e.g. $\beta$-spodumene solid solutions, spinels, cristobalite, . . .). Their constitution has heavy consequences on the properties of glass-ceramics. The $\beta$-quartz compositions within the $Li_2O$-MgO-ZnO-$Al_2O_3$-$SiO_2$ system which contains more than 2.5 wt% $Li_2O$ are currently used for commercial glass-ceramics because they produce low-expansion $\beta$-spodumene bodies. Indeed, the $\beta$-quartz type crystals transform mainly into $\beta$-spodumene solid solution and some minor phases such as spinels on heating.

The objective of the present study is to extensively characterize the microstructure of a LAS-type parent glass and two glass-ceramics by various characterization methods at different scales. This work does not discuss the crystallization process but exhibits and compares the microstructure of two different glass-ceramics produced from the same parent glass by two different crystallization heat-treatments. This study has been performed in view of interpreting the relaxation mechanical phenomena observed in these materials [16, 17].

## 2. Experimental procedure

### 2.1. Materials

The studied materials are a parent glass A and two glass-ceramics, B and C, provided by Corning Europe Inc.. These three materials are derived from the LAS system and have the same chemical composition (Table I), which is approximately (wt %): $SiO_2$ : 70, $Al_2O_3$ : 20, $Li_2O$+MgO+ZnO : 6, $TiO_2$+$ZrO_2$ : 4. The main components are $SiO_2$, $Al_2O_3$ and $Li_2O$, therefore, these materials belong to a LAS-type complex system. Various oxides have been added to the basic glass composition. $Li_2O$ is partially substituted by MgO and ZnO in order to improve the parent glass work and melting properties while lowering the cost of materials. The other minor components, such as BaO, $Na_2O$ and $K_2O$, can modify the glass-ceramic properties to a certain extent; for example, BaO acts on the material transparency. $TiO_2$ and $ZrO_2$ are the nucleating agents.

TABLE I Chemical composition (wt % and mol %) of the parent glass A and the glass-ceramics B and C determined by ICP spectrometry

| | wt % | | | mol % | | |
|---|---|---|---|---|---|---|
| | A | B | C | A | B | C |
| $SiO_2$ | 70.69 | 70.92 | 71.46 | 74.9 | 75.08 | 75.75 |
| $Al_2O_3$ | 18.04 | 18.16 | 18.13 | 11.2 | 11.31 | 11.30 |
| $Li_2O$ | 3.44 | 3.29 | 3.11 | 7.3 | 6.99 | 6.61 |
| MgO | 0.99 | 1.09 | 1.04 | 1.6 | 1.72 | 1.64 |
| ZnO | 1.22 | 1.36 | 1.39 | 1.1 | 1.22 | 1.25 |
| $TiO_2$ | 2.51 | 2.07 | 2.32 | 2 | 1.64 | 1.85 |
| $ZrO_2$ | 1.35 | 1.52 | 1.39 | 0.7 | 0.78 | 0.72 |
| $Na_2O$ | 0.44 | 0.82 | 0.51 | 0.45 | 0.84 | 0.52 |
| $K_2O$ | 0.66 | 0.17 | 0.09 | 0.44 | 0.11 | 0.06 |
| BaO | 0.73 | 0.68 | 0.67 | 0.3 | 0.28 | 0.28 |
| MnO | 0.01 | 0.02 | 0.02 | 0.01 | 0.02 | 0.01 |
| CaO | — | — | 0.04 | — | — | 0.04 |

Glass A is transparent and yellowish and its glass transition temperature is around 700°C. After an annealing around 650°C intended to eliminate the stresses, the parent glass A is submitted to industrial crystallization heat-treatments which result in glass-ceramics B and C. According to Corning Europe Inc., glass A is progressively heated up to about 700°C and then the heating rate is reduced until the nucleation stage occurs ( 800°C). Once the nucleation is achieved, the temperature is quickly increased up to the crystalline growth stage, which is around 900–930°C for glass-ceramic B and at higher temperature (1100°C–1150°C) for glass-ceramic C. Glass-ceramic B is transparent and brownish while glass-ceramic C is opaque and white.

### 2.2. Structural characterization techniques

Different techniques have been used for the characterization of the three materials.

The Differential Thermal Analysis (DTA) has been applied to determine approximately the crystallization temperature of glass A and consequently the nature of the precipitated phase. DTA analysis were performed with a Netsch thermal analyser (STA 409EP) between 20°C and 1200°C with a heating rate of 10°C/min. The bulk or powder samples were put in $Al_2O_3$ crucibles.

The X-Ray Diffraction (XRD) has been used to identify the crystalline phases present in the glass-ceramics and more particularly to determine the nature and the chemical composition of the solid solutions. XRD experiments were performed on bulk samples with a type F Siemens diffractometer operating at 45 kV and 20 mA with a $CuK_\alpha$ radiation ($\lambda_{K\alpha 1} = 1.5406$ Å) and a Ni filter, which allows a sample rotation $\theta$ coupled with a detector rotation $2\theta$.

Scanning Electron Microscopy (SEM) has been used to study the glass-ceramics morphology, the grain size and distribution in the residual glassy matrix. The samples were first cut and mechanically ground. A light HF etching is required for revealing the crystallites. The glass-ceramics B and C were immersed in a 2% HF solution during 1 min in an ultrasonic bath. Then the samples were plunged into a rinsing bath ($H_2O$ + 10% acetone) to stop etching. For SEM observations, the glass-ceramic samples were gold-coated and then observed with a JSM 600 microscope operating at 25 kV.

Transmission Electron Microscopy (TEM), owing to its high resolution, permits a more detailed microstructural characterization. Moreover, the identification of nanocrystalline precipitates is made possible by electron micro-diffraction. In order to prevent sample

damage and structural modifications due to ionic beam technique, thin foils have been prepared by ultramicrotomy [17] with a "Super Nova" Reichert Jung ultramicrotom and put on a carbon-coated copper grid. Glass-ceramic samples were then observed in a Philips CM20 TEM operating at 200 kV or a JEOL 3010 TEM equipped with Energy Dispersive X-ray Spectrometry (EDS). EDS allows to identify the nature and chemical composition of precipitated phases.

Fourier Transform Infrared (FTIR) spectroscopy has been used in order to grasp the LAS-type glass and glass-ceramic fine structure; it also allows to highlight structural modifications linked with crystallization by comparing glass and glass-ceramic FTIR spectra. Materials were fine powdered and mixed with KBr and then pressed to form pellets. FTIR spectra were measured at room temperature between 400 and 4000 $cm^{-1}$ on pellets using a BOMEN Fourier Transform Infrared spectrometer.

## 3. Results and discussion

### 3.1. Microstructure of glass-ceramics by SEM examinations

Glass-ceramic B, whose main crystalline phase is a $\beta$-quartz solid solution (see Section 3.2.1.), is composed of crystallites of approximately 100 nm in size (Fig. 1). In accordance with the literature [5,10,18–20], this glass-ceramic primarily composed of $\beta$-quartz solid solution crystals is very fine grained (50–100 nm), which can also explains its transparency even when high crystallized. These small crystals are generally conglomerated in clusters. As shown in Fig. 1, the vitreous interstitial phase is relatively limited but uniformly distributed and forms a thin vitreous film (<10 nm).

In glass-ceramic C, which has been submitted to a heat-treatment at higher temperature and contains mainly $\beta$-spodumene solid solution (see 3.2.1.), the crystals are much larger than in glass-ceramic B (Fig. 2). This is an essential feature [10, 18, 21] which can explain the opacity of glass-ceramic C. These grains have an irregular shape and do not present particular orientation. The intergranular contact seems to be sizeable; the reduced glassy phase, whose mean thickness is 150 nm, is not uniformly distributed between the grains. As shown in Fig. 2, besides these main crystals, there are other little particles which are probably secondary phase crystals (spinels and $TiZrO_4$ identified by XRD-see Section 3.2.1.).

So, the comparison between glass-ceramics B and C, crystallized from the same parent glass, shows the essential influence of crystallization heat-treatment temperature on the glass-ceramic morphology.

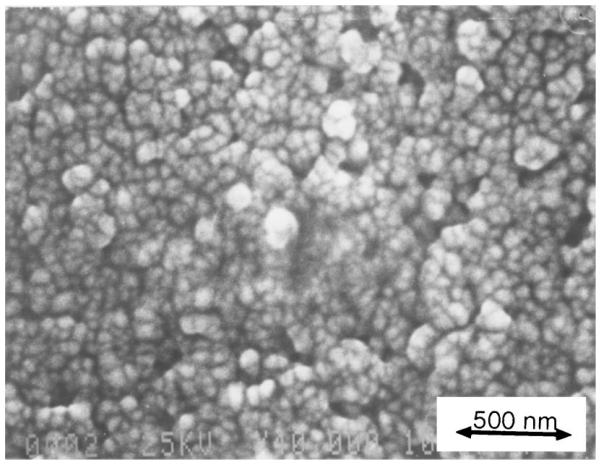


*Figure 1* SEM migrography of glass-ceramic B.

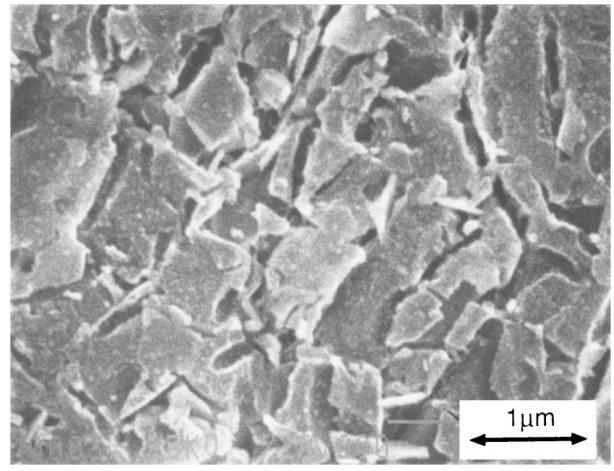


*Figure 2* SEM migrography of glass-ceramic C.

### 3.2. Phase identification

#### *3.2.1. XRD*

First, we have noticed that the samples of materials A, B and C studied by XRD showed a blackening of the irradiated part [17].

The XRD pattern of material A is characterized by a diffuse halo centered at $2\theta = 22.5^\circ$ which confirms that material A is a non-devitrificated glass. However, if there are some crystallites in material A, they are too small (<10 nm) to give a coherent XRD pattern.

The XRD pattern of glass-ceramic B (Fig. 3) shows well defined lines on the range $2\theta < 70^\circ$.

The XRD pattern of glass-ceramic C (Fig. 4) shows many diffraction lines, often weak. The most intense ones are located at relatively low angles $2\theta < 50^\circ$.

The diffraction lines with their relative intensities obtained after background subtraction for glass-ceramics B and C are given in Table II and Table III respectively.

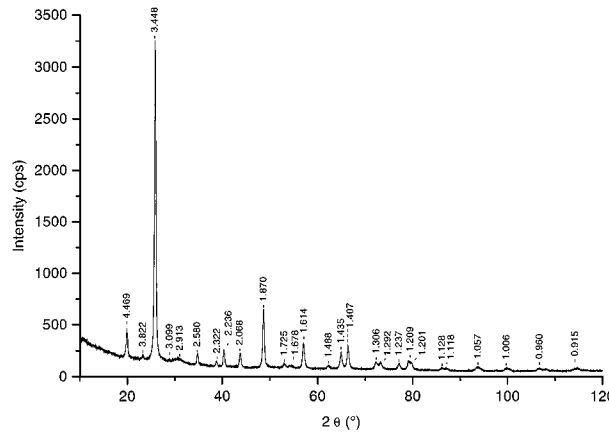


*Figure 3* XRD pattern of glass-ceramic B with lattice spacings.

TABLE II XRD data relative to glass-ceramic B

| $d_{experimental}$ (Å) | $I/I_o$ | $hkl$ | $d_{calculated}$ (Å) |
|---|---|---|---|
| 4.4686 | 9.15 | 100 | 4.471 |
| 3.8217 | 1.79 | $\beta$-spod ss | |
| 3.4481 | 100 | 101 | 3.453 |
| 3.0994 | 0.62 | $\beta$-spod ss | |
| 2.9136[a] | 1.43 | $TiZrO_4$ | |
| 2.5800 | 3.48 | 110 | 2.581 |
| 2.3224 | 1.70 | 102 | 2.322 |
| 2.2358 | 5.32 | 200 | 2.236 |
| 2.0678 | 4.40 | 201 | 2.068 |
| 1.8700 | 18.28 | 112 | 1.872 |
| 1.7245 | 1.28 | 202 | 1.726 |
| 1.6783 | 0.76 | 103 | 1.679 |
| 1.6137 | 8.04 | 211 | 1.614 |
| 1.4885 | 1.26 | 300 | 1.490 |
| 1.4353 | 5.37 | 212 | 1.435 |
| 1.4071 | 7.24 | 203 | 1.407 |
| 1.3063 | 2.31 | 302 | 1.307 |
| 1.2918 | 2.50 | 220 | 1.291 |
| 1.2366 | 2.10 | 213 | 1.236 |
| 1.2091 | 2.91 | 311 | 1.209 |
| 1.2006 | 2.30 | 114 | 1.202 |
| 1.1281 | 0.89 | 312 | 1.128 |
| 1.1184 | 0.63 | 400 | 1.118 |
| 1.0570 | 1.49 | 124 | 1.059 |
| 1.0063 | 1.17 | 321 | 1.008 |
| | | 115 | 1.002 |
| 0.9606 | 0.8 | 141 | 0.960 |
| 0.9153 | 0.99 | 134 | 0.916 |

*hkl*: Miller indices for the solid solution of $\beta$-quartz structure.
$\beta$-spod ss: $\beta$-spodumene solid solution.
[a] :bad resolved peak.

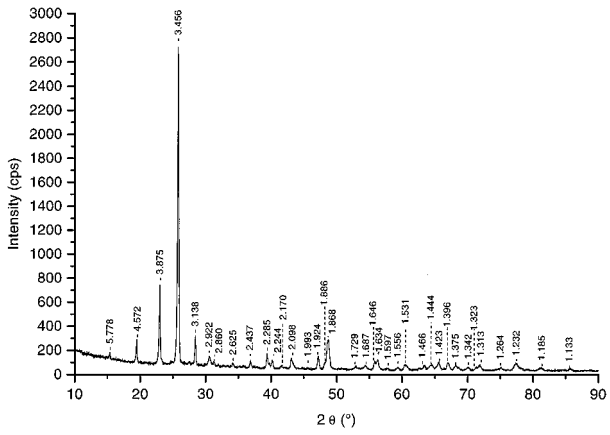


*Figure 4* XRD pattern of glass-ceramic C with lattice spacings.

According to the XRD spectra of glass-ceramics B and C, the amorphous contribution seems to be reduced but the quantitative determination of the crystalline and amorphous phases is very difficult [17, 22]; it can only be asserted that glass-ceramics B and C are very crystallized materials with a residual glassy phase. By comparison of the glass-ceramic B and C patterns, it appears that glass-ceramic C is more crystallized (around 90%) than B (<90%).

Although the glass-ceramics B and C have a complex chemical composition, their different crystalline phases have been identified from the XRD data.

*3.2.1.1. Glass-ceramic B.* First, by comparison with patterns of lithium aluminosilicates, such as

TABLE III XRD data relative to glass-ceramic C

| $d_{experimental}$ (Å) | $I/I_o$ | $hkl$ | $d_{calculated}$ (Å) |
|---|---|---|---|
| 5.7781 | 1.85 | 101 | 5.774 |
| 4.5719 | 7.16 | 111 | 4.572 |
| 3.8750 | 24.87 | 102 | 3.878 |
| 3.4565 | 100 | 201 | 3.460 |
| 3.1377 | 9.26 | 211 | 3.141 |
| 2.9221 | 3.21 | $TiZrO_4$ | |
| 2.8604 | 1.70 | $ZnAl_2O_4$ | |
| 2.6249 | 1.50 | 113 | 2.625 |
| 2.4375 | 2.36 | (Mg, Zn)$Al_2O_4$ | |
| 2.2855 | 4.04 | 222 | 2.286 |
| 2.2438 | 2.65 | 213 | 2.244 |
| 2.1699 | 0.88 | 104 | 2.169 |
| 2.0982 | 2.96 | 312 | 2.099 |
| 1.9928 | 0.46 | 223 | 1.991 |
| 1.9244 | 4.19 | 303 | 1.924 |
| 1.8865[a] | 2.30 | 322 | 1.888 |
| 1.8685 | 9.41 | 400 | 1.872 |
| | | 313 | 1.864 |
| 1.7291 | 1.14 | 402 | 1.730 |
| 1.6871 | 1.48 | 412 | 1.686 |
| 1.6459 | 2.50 | 421 | 1.646 |
| | | 332 | 1.645 |
| 1.6343 | 2.98 | 314 | 1.637 |
| | | 205 | 1.632 |
| 1.5966 | 0.53 | 215 | 1.595 |
| 1.5565 | 0.82 | 413+(Zn,Mg)$Al_2O_4$ | 1.557 |
| 1.5314 | 1.58 | 324 | 1.531 |
| 1.4660 | 1.70 | 305 | 1.467 |
| 1.4443 | 2.09 | 404 | 1.443 |
| 1.4229 | 2.68 | 502 = 342 +(Zn,Mg)$Al_2O_4$ | 1.422 |
| 1.3960 | 2.18 | 512 | 1.397 |
| 1.3748 | 1.74 | 521 | 1.374 |
| 1.3423 | 0.99 | 503 = 343 | 1.342 |
| 1.3229 | 1.09 | 440 | 1.324 |
| | | 513 | 1.321 |
| 1.3135 | 1.54 | 226 | 1.312 |
| 1.2639 | 0.92 | 335 | 1.265 |
| | | 523 | 1.263 |
| 1.2320 | 2.13 | 514 | 1.232 |
| | | 610 | 1.231 |
| 1.1849 | 1.02 | 524 | 1.185 |
| | | 260 | 1.184 |
| 1.1331 | 1.04 | 008 | 1.134 |
| | | 452 | 1.132 |

*hkl*: Miller indices for the solid solution of $\beta$-spodumene.
[a]: shoulder.

$Li_xAl_xSi_{1-x}O_2$ with $x \sim 0.29$ (JCPDS 40-73) [23], $LiAl(SiO_3)_2$ (JCPDS 31-706), $Li_2Al_2Si_3O_{10}$ (JCPDS 25-1183) and $Li_{1.01}(AlO_2)_{1.03}(SiO_2)_{1.16}$ (JCPDS 45-467), the main phase of B has been identified as a $\beta$-quartz solid solution of $Li_2O{\cdot}Al_2O_3.nSiO_2$ type. However, the glass-ceramic B also contains Mg and Zn, and its diffraction pattern is rather close to the diffractograms of some magnesium aluminosilicates and particularly of $MgAl_2Si_4O_{12}$ (JCPDS 25-716), and also of the zinc aluminosilicate ($Zn_{0.75}Al_{1.5}Si_{1.5}O_6$) (JCPDS 32-1455). All these compounds, whose pattern exhibits strong analogies with the glass-ceramic B one, have a stuffed $\beta$-quartz structure with lattice parameters close to the $\beta$-quartz ones. The main phase of B is therefore a stuffed $\beta$-quartz solid solution, derived from LAS system, where Mg and Zn are substitutes for Li: $Zn_{z/2}Mg_{y/2}Li_{x-(y+z)}Al_xSi_{1-x}O_2$ (or $Zn_zMg_yLi_{(2-y-z)}O{\cdot}Al_2O_3{\cdot}nSiO_2$).

The comparison of XRD data with those of known lithium aluminosilicates, such as $Li_{0.29}Al_{0.29}Si_{0.71}O_2$ [23], $LiAlSi_2O_6$ [24] and $Li_2Al_2Si_3O_{10}$ [25], allows to index the spectral lines relative to the solid solution (Table II) on the basis of a $\beta$-quartz structure with the single $a$ and $c$ cell parameters.

The lattice parameters of the $\beta$-quartz solid solution have been calculated from the measured lattice spacings with the expression relative to the hexagonal system:

$$d_{hkl}^2 = \frac{a^2}{\frac{4}{3}(h^2 + k^2 + hk) + l^2\frac{a^2}{c^2}} \quad (1)$$

According to the criteria of Iwatsuki *et al.* [26–28], who have studied several $\beta$-eucryptite solid solutions, the high intensity and well defined lines located between 40 and 70°, namely the (200), (201), (212) and (203) lines have been selected for lattice parameters determination. The $a$ and $c$ values have been calculated using the $d$-spacings for all the various pairs of these four lines respectively. The mean values of the cell parameters of the main crystalline phase of B, that is to say the stuffed $\beta$-quartz solid solution with hexagonal structure, are: $a = (5.163 \pm 0.002)$ Å and $c = (5.435 \pm 0.006)$ Å. There is a good agreement between the calculated and the experimental lattice spacing values (see Table II), which indicates that the calculated $a$ and $c$ parameters are correct.

In glass-ceramic B diffraction pattern, some lines do not correspond to a $\beta$-quartz solid solution and then show the presence of secondary phases. The two peaks observed in diffraction pattern of B ($d = 3.822$ Å and $d = 3.099$ Å) indicate the presence of a $\beta$-spodumene solid solution, as a secondary phase in the glass-ceramic B, which is confirmed by the observations of different authors [8, 27, 29]. The lattice parameters of this tetragonal solid solution ($a = 7.39$ Å and $c = 8.93$ Å) have been calculated from the lattice spacing of these two lines with

$$d_{hkl}^2 = \frac{a^2}{h^2 + k^2 + l^2\frac{a^2}{c^2}} \quad (2)$$

The wide and bad defined low intensity peak, about 2.913 Å, which is characteristic of neither $\beta$-quartz solid solution nor $\beta$-spodumene solid solution, corresponds to the strongest reflection of $TiZrO_4$, the (111) line whose lattice spacing is 2.93 Å (JCPDS 34-415). According to the studies performed on the crystallization of lithium aluminosilicate glasses containing $TiO_2$ and $ZrO_2$ [5, 6, 20, 30, 31], the $TiZrO_4$ crystallites constitute the heterogeneous nuclei from which the crystalline growth of $\beta$-quartz solid solution takes place. After crystallization, $TiZrO_4$, remains as nanocrystallites inside the $\beta$-quartz solid solution crystals, as it will be shown in the TEM analysis.

The quantitative determination of the main and secondary phases is not possible because for one line there is the contribution of these two phases. Indeed, in agreement with Roy's observations [29], the LAS system $\beta$-quartz and $\beta$-spodumene solid solutions have very similar diffraction patterns. However, the low intensity of the (102) line of the $\beta$-spodumene solid solution indicates that the amount of this secondary phase is very low. The $TiZrO_4$ seems to be also present in a low amount in glass-ceramic B.

So the main crystalline phase of glass-ceramic B is a stuffed $\beta$-quartz solid solution of $(ZnO,MgO,Li_2O)\cdot Al_2O_3\cdot nSiO_2$ type having hexagonal structure with $a = (5.163 \pm 0.002)$ Å and $c = (5.435 \pm 0.006)$ Å. The secondary phases have been identified as a tetragonal $\beta$-spodumene solid solution ($a = 7.39$ Å and $c = 8.93$ Å) and $TiZrO_4$.

*3.2.1.2. Glass-ceramic C.* With regard to both line sequence and intensity ratio, the glass-ceramic C pattern is very close to the diffractograms of lithium aluminosilicates with $\beta$-spodumene structure such as $LiAlSi_2O_6$ (JCPDS 35-797), $LiAlSi_3O_8$ (JCPDS 35-794) [32], $\beta$-spodumene solid solution $(Li_{0.23}Na_{0.06})Al_{0.29}Si_{0.71}O_2$ derived from (Li,Na)-Y zeolithe [23]. It is more particularly very close to the $Li_{0.6}Al_{0.6}Si_{2.4}O_6$, ($Li_xAl_xSi_{1-x}O_2$ with $x = 0.20$) phase (JCPDS 21-503) studied by Ostertag *et al.* [33]. The main crystalline phase of glass-ceramic C has been identified as a $\beta$-spodumene solid solution of general composition $Li_xAl_xSi_{1-x}O_2$ with $x \leq 0.33$ (or $Li_2O\cdot Al_2O_3 nSiO_2$ with $n \geq 4$).

The line identification and indexation (Table III) has been achieved by comparison with the diffraction data of keatite (JCPDS 13-26) and the previous aluminosilicates and more particularly $Li_2O\cdot Al_2O_3\cdot 8SiO_2$ [33], by taking into account a tetragonal $\beta$-spodumene like structure ($P4_32_12$ group space). The lattice parameters ($a$ and $c$) of the tetragonal $\beta$-spodumene solid solution have been determined from the measured lattice spacings by using formula (2). By relying on Fukasawa *et al.* analysis for the $\beta$-spodumene solid solution in glass-ceramics [34] and by using the same criteria than for the glass-ceramic B, the four lines (303), (503), (324) and (113) have been used. The lattice parameters calculated by this way are: $a = 7.488 \pm 0.005$ Å and $c = 9.067 \pm 0.008$ Å. The lattice spacings calculated from $a$ and $c$ values mentioned just above coincide quite well with the experimental values (Table III), which proves the validity of the lattice constant values.

In the diffraction pattern, the presence of three low intensity lines ($d \sim 2.921$ Å, $d = 2.860$ Å and $d = 2.437$ Å) but quite well defined and not characteristic of the $\beta$-spodumene solid solution, implies the existence of secondary phases in glass-ceramic C. The line ($d \sim 2.921$ Å) corresponds to the highest intensity line (111) of $TiZrO_4$, but as the $TiZrO_4$ content in glass-ceramic C is low, the other lines are not visible. The measured lines ($d = 2.437$ Å and $d = 2.860$ Å) correspond respectively to the (111) and (220) lines of the Mg and Zn spinels ($MgAl_2O_4$ and $ZnAl_2O_4$) or of a gahnospinel (Zn, Mg) $Al_2O_4$, since a complete solid solution can exist between $ZnAl_2O_4$ and $MgAl_2O_4$ [35]. The presence of gahnospinels is confirmed by Tereschenko *et al.* [36] and Ray and Muchow [8] who have studied the crystallization and the transformation

of the LAS $\beta$-quartz solid solution containing ZnO and MgO into $\beta$-spodumene solid solution; during the metastable $\beta$-quartz solid solution transformation, Zn and a part of Mg are expelled from the structure and form Mg and Zn spinels (Mg $Al_2O_4$ and $ZnAl_2O_4$) or gahnospinels (Zn, Mg) $Al_2O_4$.

So the main crystalline phase of glass-ceramic C is a tetragonal $\beta$-spodumene solid solution with $a = 7.488 \pm 0.005$ Å and $c = 9.067 \pm 0.008$ Å. The secondary phases present in a low amount have been identified as $TiZrO_4$, and, Mg and Zn spinels or gahnospinels.

### 3.2.2. DTA

The DTA curve after base line subtraction for powdered glass A is given in Fig. 5. The main feature is an exothermic maximum at 860°C corresponding to the $\beta$-quartz solid solution phase crystallization and, so, to the glass A crystallization in glass-ceramic B, as confirmed by several studies [10, 21]. However, the transformation of glass-ceramic B into glass-ceramic C, that is to say the stuffed $\beta$-quartz crystalline phase transformation into $\beta$-spodumene solid solution, does not appear on the DTA recording. Nevertheless, there is no doubt about the occurrence of the transformation because, after analysis, the sample was not translucent anymore but was white and opaque, which is a feature of the glass-ceramic C. As previously mentioned, except the stoichiometric stable $\beta$-eucryptite phase, the L.A.nS type stuffed $\beta$-quartz solid solutions with $n \geq 3.5$ are metastable and during the heating at enough high temperature, they transform into stable crystalline phases, which are $\beta$-spodumene solid solutions [4, 9, 10, 21, 37].

DTA analyses have also been performed on a glass-ceramic B sample in order to study more precisely the transformation of the glass-ceramic B into glass-ceramic C. The initially transparent sample became opaque and white, which indicates that the transformation of glass-ceramic B into C has occurred during experiments. On the DTA spectrum (Fig. 6), contrary to glass crystallization, there is no well defined peak but only a very weak exothermic phenomenon around 1050°C, in agreement with Li's results [38] concerning the $LiAlSi_2O_6$ hexagonal $\beta$-quartz phase transformation into tetragonal keatite phase. This observation shows that this conversion involves not much energy and it is likely that atoms undergo small position changes. Moreover, it seems that the transformation does not occur at a well precise temperature but extends over a temperature range. There is a great discrepancy in the literature data [18, 21, 36] for the transformation point temperature ranging between 950 and 1050°C. The higher $n$ in L.A.nS solid solution, the lower the transformation temperature [8]. Several analyses performed on glass-ceramic B show that increasing heating rate shifts the B into C transformation towards higher temperatures : the peak is located around 970°C for a rate of 2°C/min, near 1000°C for 5°C/min and around 1050°C for a rate of 10°C/min.

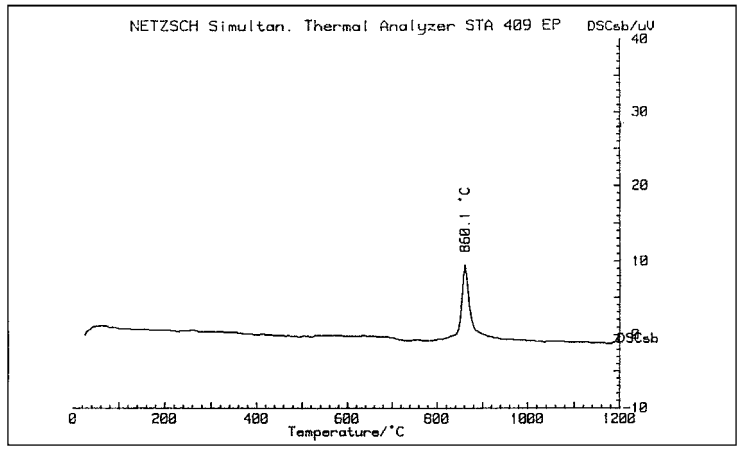


*Figure 5* DTA spectrum of glass A (heating rate: 10°C/min).

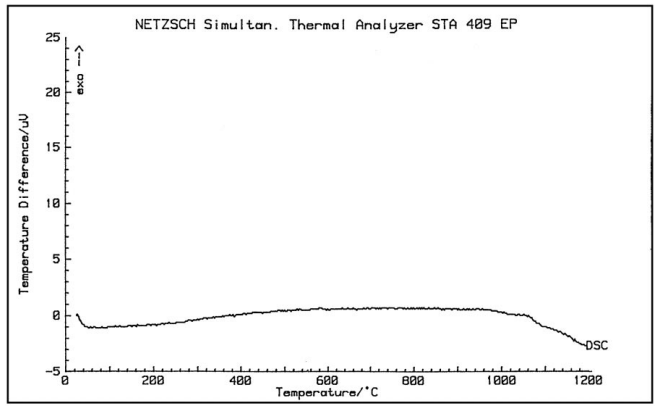


*Figure 6* DTA spectrum of glass-ceramic B (heating rate: 10°C/min).

The presence of $\beta$-quartz solid solution as the main crystalline phase in glass-ceramic B is confirmed by the DTA measurements.

### 3.2.3. TEM

*3.2.3.1. Glass A.* Fig. 7 depicts a low magnification micrograph of the parent glass which indicates an homogeneous and essentially featureless morphology, although at higher magnification (Fig. 8) a fine scale morphology is revealed. This heterogeneous appearance is likely due to intensity modulation linked with phase separation. The size of the glass-in-glass demixtion is smaller than 10 nm (Fig. 8). Indeed, apparently transparent and homogeneous glasses may contain separated domains of a few nanometers, the finest phase separation being from 3 nm to 5 nm [19]. For a LAS-type Corning glass close to glass A in composition, Ramos [20] has observed the existence of glass-in-glass phase separation with a characteristic size of nearly 7 nm. The corresponding electron diffraction analysis shows a glassy halo, which is in accordance with the XRD results and indicates that material A is amorphous.

Although glass A is mainly amorphous, it contains some very localized partially crystallized zones with crystallites smaller than 5 nm, which have been identified by microdiffraction and dark fields as being essentially $TiZrO_4$ with trace of $TiO_2$ and $\beta$-quartz solid solution (Fig. 9). So glass A has undergone a slight devitrification; either the crystallites have appeared during glass elaboration or during the annealing to release stresses, or they have been formed during ultramicrotome cut.

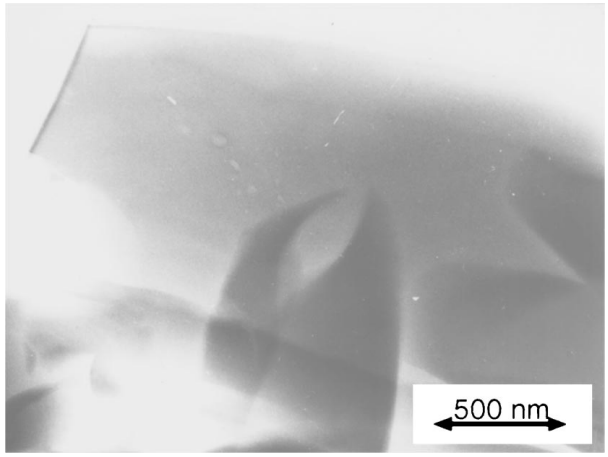


*Figure 7* TEM micrography of glass A: general view.

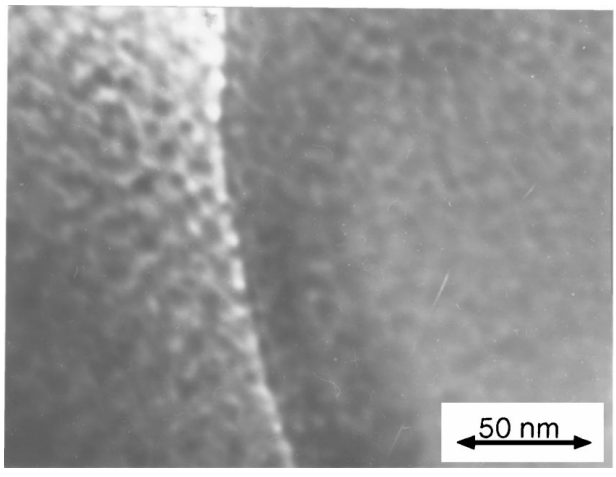


*Figure 8* High magnification TEM micrography of glass A.

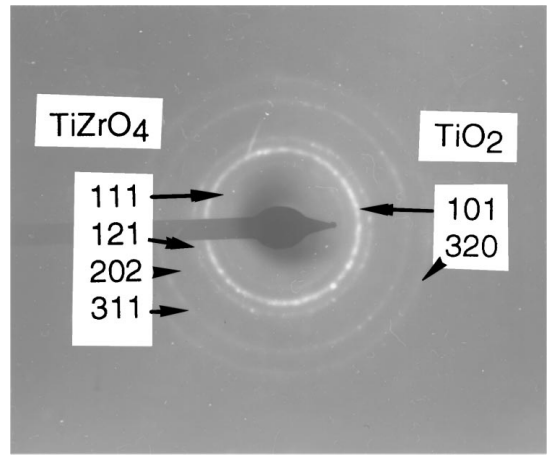


*Figure 9* Electron diffraction pattern of a small crystallized area in glass A.

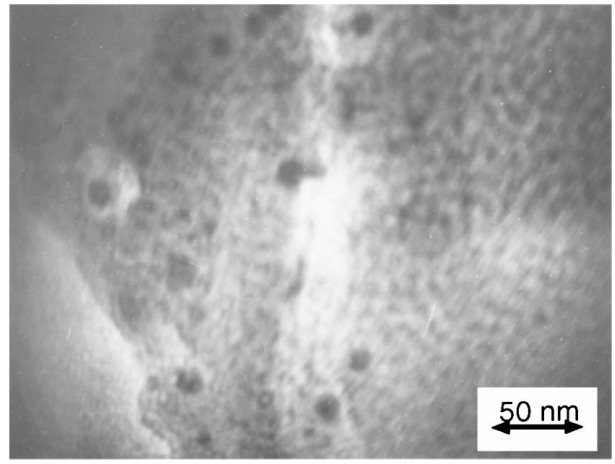


*Figure 10* In situ TEM micrography of glass A at 850°C.

The structural evolution of an initially glassy zone has been studied by an in situ heat treatment of glass A, from room temperature up to 920°C with a heating rate of 20°C/min. The material remains amorphous and no apparent change is observable up to 827°C, temperature at which embryos smaller than 10 nm appear (Fig. 10). During the heating up to 860°C, these nuclei remain and even grow a little. Above 860°C, they progressively disappear under the electron beam and as fast as the beam is condensed. Back to room temperature the structure is the same than before heating. So, the $TiZrO_4$ nuclei, which are likely to form during a temperature holding above 810°C and which, according to the literature [10, 20, 30], make up the essential nuclei for the further crystallization of the stuffed $\beta$-quartz phase, have not probably reached here the critical size during the fast temperature rise and have disappeared. Even if $TiZrO_4$ is present in the glassy matrix, it can not be identified because its main diffraction ring corresponding to $d_{111} = 2.93$ Å would be concealed in the area of transmitted beam. The nanocrystallites formed

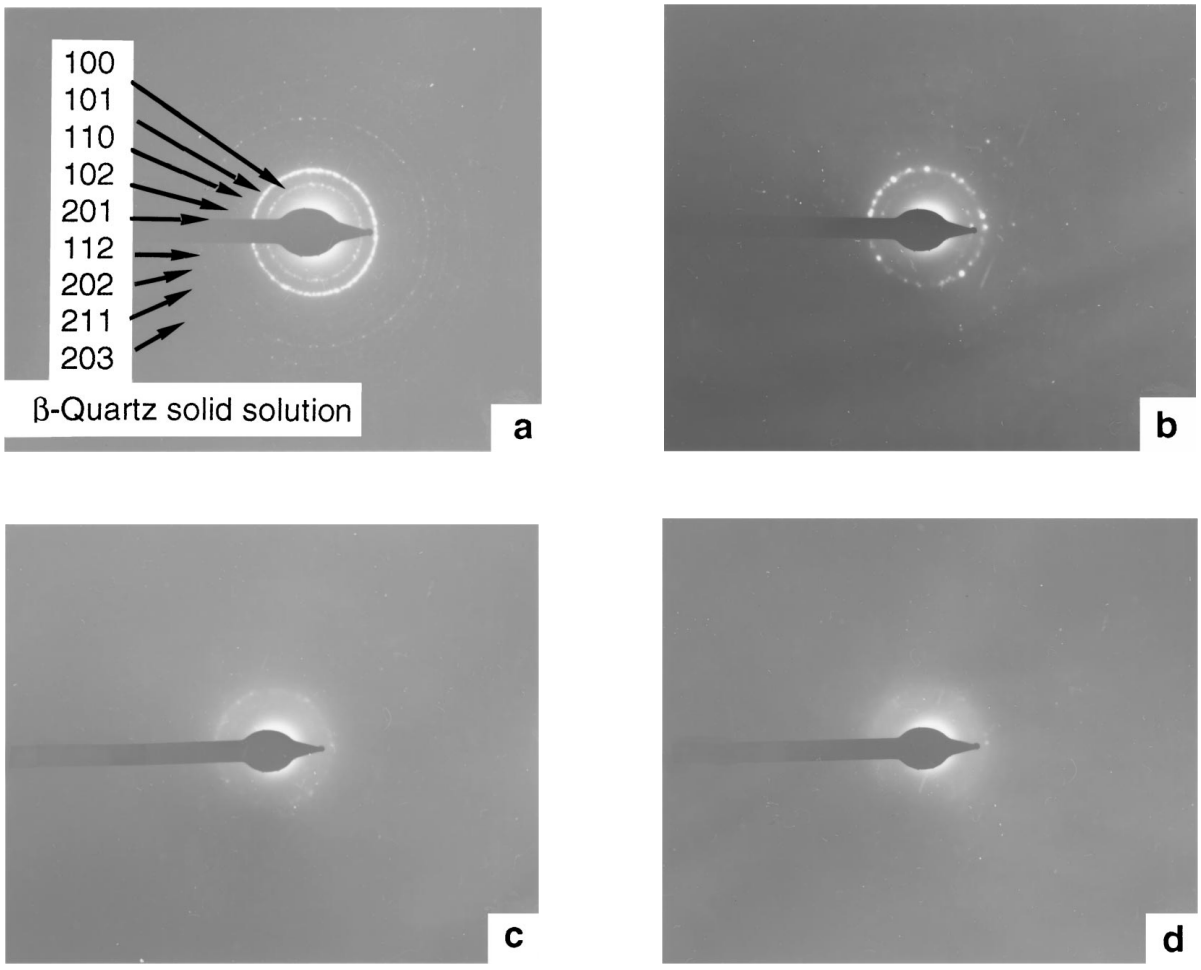


*Figure 11* Room temperature electron diffraction patterns of glass-ceramic B at different times: a) initial exposure (0 s), b) 15 s, c) 30 s, d) 45 s.

above 827°C, which become amorphous under the electron beam may be $\beta$-quartz solid solution crystallites [20, 39, 40].

*3.2.3.2. Glass-ceramic B.* Sample B is composed of lots of crystallites of approximately 30–40 nm in size giving diffraction rings (Fig. 11a) and identified as a stuffed $\beta$-quartz solid solution. However, during TEM observations, glass-ceramic B undergoes a rapid degradation under the electron beam, which makes the examination difficult. Such a phenomenon has already been noted for LAS-type glass-ceramic primarily composed of a stuffed $\beta$-quartz solid solution [20, 39, 40]. This amorphization occurs very quickly, from 10 s to 1 min according to the beam condensation. Representative electron diffraction micrographs of sample B taken at different times (0 s, 15 s, 30 s and 45 s respectively) are represented in Fig. 11a,b,c,d. Contrary to XRD results, $TiZrO_4$, which is nevertheless known to be stable under electron beam, has not been detected, its volume fraction being probably too small and its distribution non homogeneous.

*3.2.3.3. Glass-ceramic C.* A global view at relatively low magnification (Fig. 12) depicts grain fragments of glass-ceramic C, which are heterogeneous and contain crystallites between 10 and 100 nm in size. The electron diffraction of one fragment (Fig. 13) indicates that it is a $\beta$-spodumene solid solution grain, which confirms the XRD results.

There is also a degradation of the $\beta$-spodumene solid solution under the electron beam (Fig. 14a,b,c) but it is slower than for glass-ceramic B (several minutes between two successive micrographs). However, the crystallites distributed in the grain are stable under the electron beam. The biggest ones are parallelepipedic, about 100 nm in length (Fig. 15: bright field) whereas the smallest ones are only $\sim$10 nm in size, but both have been identified by electron diffraction as $TiZrO_4$ crystallites. This fact is in agreement with EDS analysis which has revealed that Ti, Zr and O are the main elements. The simultaneous presence of these two kinds of $TiZrO_4$ crystallites has also been observed by Barry *et al*. [41].

## 3.3. Composition of the main crystalline phases of the glass-ceramics

### *3.3.1. Glass-ceramic B: $\beta$-quartz solid solution*

The XRD data allow the quantitative determination of the stuffed $\beta$-quartz solid solution which is of the following type: $Zn_{z/2}Mg_{y/2}Li_{x-(z+y)}Al_xSi_{1-x}O_2$ or $[Zn_{z/x}Mg_{y/x}Li_{2(1-(y+z)/x)}]O{\cdot}Al_2O_3{\cdot}nSiO_2$ with $n = 2(1-x)/x$ and mol % $SiO_2 = 100(1-x)$.

Contrary to the LAS [8, 15, 27], MAS [42], MLAS ($MgO\text{-}Li_2O\text{-}Al_2O_3\text{-}SiO_2$) [4, 8, 15, 26] and ZLAS

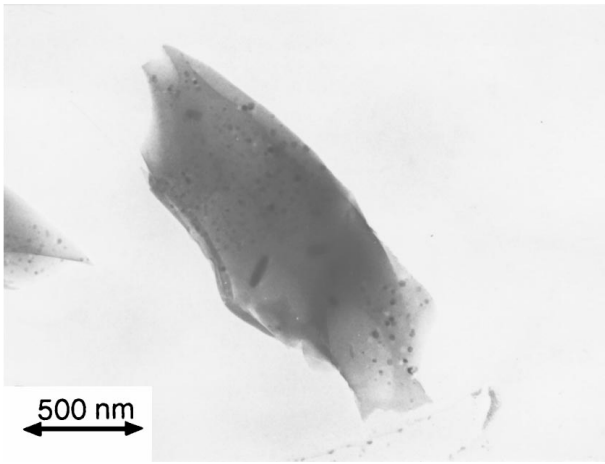


*Figure 12* General view of a glass-ceramic C fragment.

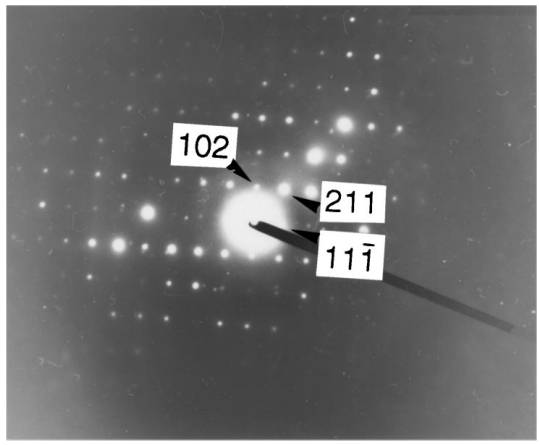


*Figure 13* Electron diffraction pattern of glass-ceramic C; $\beta$-spodumene solid solution (zone axis [$\bar{2}$31]).

($ZnO$-$Li_2O$-$Al_2O_3$-$SiO_2$) [15] systems, the $\beta$-quartz solid solution containing Mg and Zn are pseudo-quaternary systems ($SiO_2$-$LiAlO_2$-$Mg_{1/2}AlO_2$-$Zn_{1/2}AlO_2$) whose compositions can not be determined only from the lattice constants $a$ and $c$. Iwatsuki *et al*. [26] have developed a method which, in theory, allows to determine precisely the composition of a $\beta$-eucryptite solid solution containing Mg and Zn from the parameters ($a$, $c$) and from the intensity ratio of the (100) and (200) lines, but which, in practise, is difficult to be used. Moreover, as in the present case it is impossible to evaluate the (100) line intensity because of the $\beta$-spodumene secondary phase contribution to this diffraction peak, Iwatsuki's method is unsuitable. A simplifying assumption has been used: for the glass-ceramic B containing (mol%) 6.99 $Li_2O$, 1.72 MgO and 1.22 ZnO, $Li_2O$, MgO and ZnO are in the same proportion in the $\beta$-quartz solid solution as in the glass-ceramic B, which is not totally correct because a very small $Li_2O$ content contributes to the secondary minor $\beta$-spodumene phase. So $y = 0.1732x$, $z = 0.1229x$ and $y = 1.4098z$, which leads to $[Zn_{0.061x}Mg_{0.087x}Li_{0.704x}]Alx Si_{1-x}O_2$ or $[Zn_{0.123}Mg_{0.173}Li_{1.408}]O{\cdot}Al_2O_3{\cdot}nSiO_2$. A significant analyzing and comparing work [17], from the previous studies of the dependence of the lattice parameters ($a$, $c$) on the glass composition for ZLAS [15], MLAS

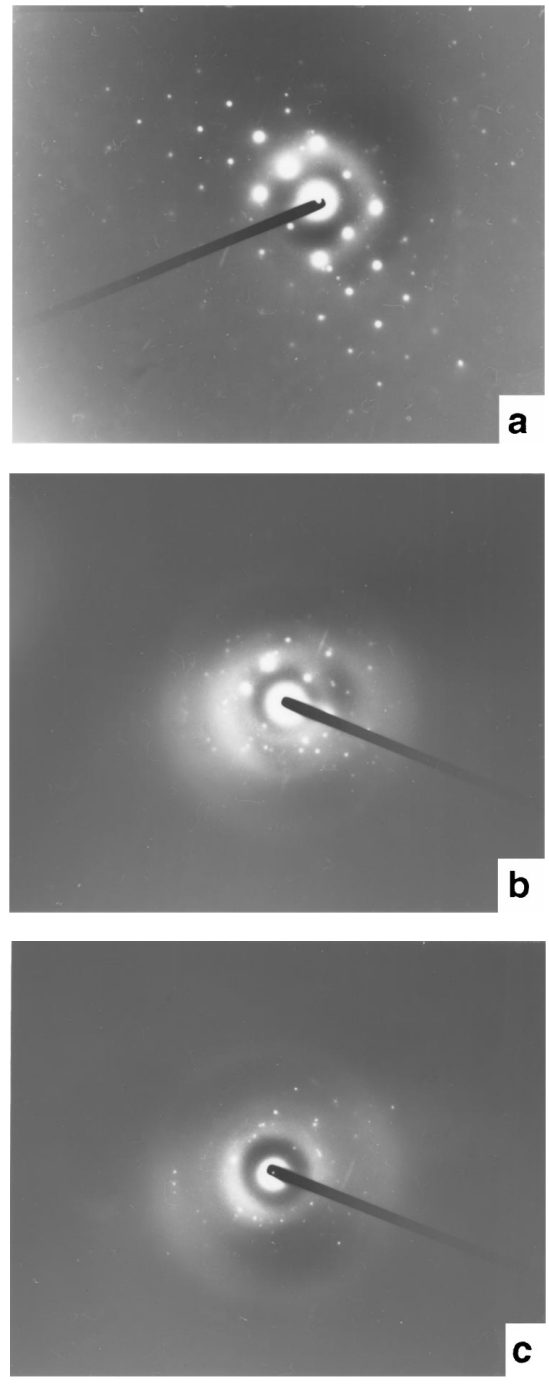


*Figure 14* a,b,c Series of electron diffraction patterns of glass-ceramic C at different times.

[8, 15, 26, 28] and ZMLAS [26] $\beta$-quartz solid solutions, has been performed to determine the composition. The $SiO_2$ contents deduced from the comparison of the solid solution lattice parameters ($a = 5.163$ Å and $c = 5.435$ Å) and, in a certain extent, from some lattice spacings ($d_{201}$, $d_{203}$) with the different literature results are summed up in Table IV.

All these results are consistent. However, the results of Iwatsuki *et al*. [26, 28] are more reliable than those of Petzoldt [15] and Ray *et al*. [8] since their study is more rigorous, lots of precautions having been taken for its achievement (such as material chemical analysis, taking into account of the $Li_2O$ evaporation and precise determination of the lattice constants). Moreover, the $\beta$-quartz solid solution of B belonging to the ZMLAS

TABLE IV $SiO_2$ content of the $\beta$-quartz solid solution of the glass-ceramic B deduced from different references

| References | | ZLAS | MLAS | | | ZMLAS |
|---|---|---|---|---|---|---|
| | | Petzoldt [15] | Petzoldt [15] | Ray [8] corrected with [28] | Iwatsuki [26, 28] | Iwatsuki [26] |
| $SiO_2$ | $n$ | 5.4–7.1 | 5.4–7.5 | 5.3–5.5 | 5.7–6 | ∼6 |
| content | $x$ | 0.22–0.27 | 0.21–0.27 | ∼0.27 | 0.25–0.26 | ∼0.25 |
| | mol % | 73–78 | 73–79 | ∼73 | 74–75 | ∼75 |

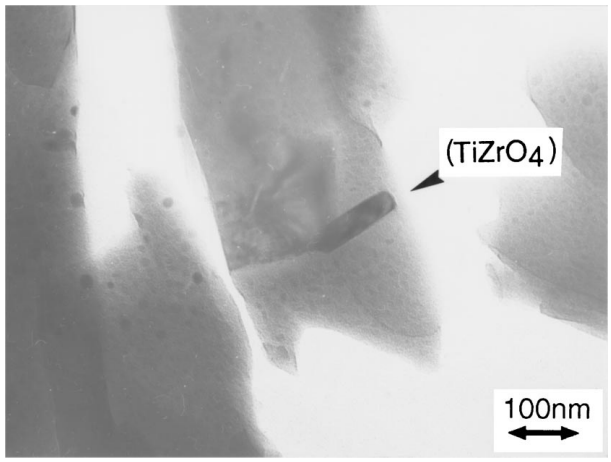


*Figure 15* Glass-ceramic C TEM micrography showing $TiZrO_4$ crystallites.

system, the $SiO_2$ content seems to be close to 75 mol%, that is to say $x \sim 0.25$ and $n \sim 6$.

So, the main crystalline phase of glass-ceramic B is a stuffed $\beta$-quartz solid solution with hexagonal lattice constants ($a = 5.163 \pm 0.002$ Å; $c = 5.435 \pm 0.006$ Å) and a chemical composition closed to: $[Zn_{0.0155}Mg_{0.02175}Li_{0.176}]Al_{0.25}Si_{0.75}O_2$ ($x \sim 0.25$) or $[Zn_{0.123}Mg_{0.173}Li_{1.408}]O{\cdot}Al_2O_3{\cdot}6SiO_2$ ($n \sim 6$)

### 3.3.2. Glass ceramic C: $\beta$-spodumene solid solution

The main phase of glass-ceramic C is a $\beta$-spodumene/keatite tetragonal solid solution of $Li_2O{\cdot}Al_2O_3{\cdot}nSiO_2$ with $n \geq 4$ also written $Li_xAl_xSi_{1-x}O_2$ with $x \leq 0.33$ ($n = 2(1-x)/x$ and mol%$SiO_2 = 100(1-x)$).

The lattice parameters of $\beta$-spodumene solid solution, determined by Skinner and Evans [32] and Ostertag *et al*. [33] in the whole existence range, are not reliable and lead to incoherent results for our solid solution. By referring to the more reliable study of Fukasawa *et al*. [34], in which the $\beta$-spodumene solid solution composition in glass-ceramic has been analyzed by XRD by measuring the lattice constants variations, the experimental $a$ and $c$ values ($a = 7.488$ Å and $c = 9.067$ Å) give $x = 0.22$ (78 mol% $SiO_2$) and $x = 0.21$ (79 mol% $SiO_2$) respectively. As the $a$ and $c$ values strongly depend on the chosen diffraction peaks, it is often more simple for a solid solution composition determination to use the change in lattice spacing of some reliable lines. By referring to Fukasawa *et al*. [34], who have established the dependence of the (303) and (503) lines on the % $SiO_2$, the $SiO_2$ content in the studied solid solution deduced from the experimental values of these two lines is (mol% $SiO_2$) 78.7.

So, the main crystalline phase of the glass-ceramic C is a tetragonal $\beta$-spodumene solid solution ($a = 7.488 \pm 0.005$ Å and $c = 9.067 \pm 0.008$ Å) with the following composition: $Li_{0.21}Al_{0.21}Si_{0.79}O_2$ or $Li_2O{\cdot}Al_2O_3{\cdot}7.5SiO_2$.

## 3.4. Fine structure of the materials

### 3.4.1. Structural data of the main crystalline phases of the glass-ceramics

*3.4.1.1. Glass-ceramic B: $\beta$-quartz solid solution.* Among the solid solutions whose structure has been fully studied, ($LiAlSi_2O_6$ III) [43] is the nearest to our solid solution $[Zn_{0.123}Mg_{0.173}Li_{1.408}]O{\cdot}Al_2O_3{\cdot}6SiO_2$ ($n \sim 6$). $LiAlSi_2O_6$ III is a stuffed $\beta$-quartz derivative with the basic $\beta$-quartz structure [35]. It has an hexagonal cell (space group: $P6_222$ or $P6_422$) with lattice parameters $a = 5.217$ Å and $c = 5.464$ Å and it contains a $LiAlSi_2O_6$ unit per cell. Its structure consists in a three-dimensional aluminosilicate network where the Si and Al atoms occupy the special 3-fold positions (3c) and their distribution in the tetrahedra is totally random. As for the lithium atoms, which are inserted in the structure to ensure the charge balance, they occupy the special 3-fold positions (3a). These three equivalent interstitial sites, located along the $c$ axis ((000), (00 1/3) and (00 2/3)) [43], are pseudo-octahedral. However, the lithium ions, randomly stuffed in these interstitial positions, are 4-fold coordinated and form a irregular tetrahedron with the four nearest neighboring oxygen atoms. Each Li tetrahedron forms two 4-membered rings with (Si,Al) tetrahedra which help to stabilize the lithium position [43]. The oxygen atoms O are in the positions 6j in the cell. The (Si,Al) tetrahedra form interconnecting 6- and 8-membered rings.

In the solid solution of glass-ceramic B, the global structure relative to the arrangement and the distribution of the different elements is probably not modified. Only a few differences in the structural parameters can exist between the solid solution of glass-ceramic B and $LiAlSi_2O_6$ III. According to the study of Chi-Tang Li [11] and of Iwatsuki *et al*. [27], the composition of $\beta$-quartz solid solution $LiO_2{\cdot}Al_2O_3{\cdot}nSiO_2$ acts on several structural parameters:

1) *the distribution of Li ions over the three equipoints (3a) of the unit cell*. The stuffed $\beta$-quartz solid solution of glass-ceramic B with $n \sim 6$ ($x = 0.25$) contains only 0.75 Li atom per cell and so, there are more unoccupied interstitial sites of rank 3 than in $LiAlSi_2O_6$ III.

2) *the lattice parameters*. For the solid solutions rich in lithium, the Li-Li distance being short, the repulsive force may be strong enough to increase the c parameter. This can explain that the lattice parameter of the solid solution of glass-ceramic B is smaller than in $LiAlSi_2O_6$ III.

3) *the (Si,Al)-O bond length [11]*. The higher the aluminium content, the longer this bond. Thus the average (Si,Al)-O distance is shorter in the solid solution of the glass-ceramic B ($n \sim 6$) than in $LiAlSi_2O_6$ III (1.641 Å).

4) *the O-O edges of the (Si,Al) tetrahedra not shared with Li tetrahedra*. The higher the aluminum content, the longer these edges [11]. So, these edges in solid solution of B are expected to be shorter than in $LiAlSi_2O_6$ III (2.706 Å).

5) *the Li-(Si,Al) distances*. The higher the $SiO_2$ content, the smaller the Li-(Si,Al) distances [11, 27] (2.624 Å for $n = 2$ to 2.595 Å for $n = 5$ [27]). Thus in the solid solution of B ($n \sim 6$), the distance will be shorter ($d < 2.595$ Å).

6) *the (Si,Al)-O-(Si,Al) angle [44]*. The higher $n$, the higher the angle; so, the solid solution of B ($n \sim 6$) has certainly a (Si,Al)-O-(Si,Al) angle higher than that of $LiAlSi_2O_6$ III (151.8°). The increase of this angle enhances the strain energy in these structures. The solid solution of B is more unstable than $LiAlSi_2O_6$ III and thus, its transformation in stuffed keatite solid solution at higher temperature is easier.

Moreover, in the solid solution of B containing Mg and Zn, the $Mg^{2+}$ ions, with ionic radius similar to the $Li^+$ one, can also insert into the interstitial sites along screw axes [7] in order to maintain the charge balance. Thus Mg substitutes for Li and consequently forms $MgO_4$ tetrahedra [26]. Zn can also take part in such structures. The Zn ions are generally located in interstitial positions in the same way as the Li and Mg ions; however, if there is an Al deficiency in the composition, Zn ions can take a 4-fold coordination. In the solid solution of B, the $Zn^{2+}$ ions are thus located in the interstitial sites.

*3.4.1.2. Glass ceramic C: β-spodumene solid solution.* Skinner and Evans [32] have studied lots of β-spodumene solid solutions of the $Li_xAl_xSi_{1-x}O_2$ series for $0.164 < x < 0.358$, obtained by glass crystallization. They stated that β-spodumene and β-spodumene solid solutions have the same space group ($P4_32_12$) and are isostructural with keatite [45]. According to Li and Peacor [46], the β-spodumene (β-$LiAlSi_2O_6$) was found to be tetragonal, space group $P4_32_12$ (or $P4_12_12$) and to have lattice parameters $a = 7.451$ Å and $c = 9.156$ Å. The unit cell of β-spodumene contains 4 formula units of $LiAlSi_2O_6$ corresponding to the 12 $SiO_2$ formula units for keatite, Al atoms randomly substituting for one third of Si atoms. The structure of the β-spodumene consists of a network arrangement of 12 $(Si,Al)O_4$ tetrahedra in the tetragonal unit cell. Of these eight form spiral chains around 4-fold screw axes $4_3$, which create channels parallel to the $c$ axis. The remaining four tetrahedra lie on horizontal diagonal 2-fold rotary axes [32] close to the screw axes $2_1$ [47]. The (Si,Al) tetrahedra form interconnecting 5-, 7-, and 8-membered rings; however, the structure is essentially made up by interlocking 5-membered rings. The interconnecting rings, quasi-pentagonal, run approximately parallel to either (100) or (010), and thus help to create zeolite-like channels. Lithium ions are stuffed into interstices in the framework to maintain charge balance. The 4 Li atoms per unit cell are distributed among 4 sites of paired sites of 8-fold positions (8b). Each Li atom occupies either of the two sites in each pair, the distance between the two sites in each pair being too short (~1.33 Å). In these sites, Li atoms are 4-fold coordinated with 4 oxygen atoms, but the tetrahedra are very distorted. Each lithium ion is located between two 5-membered rings of (Si,Al) tetrahedra, one oriented up, approximately parallel to (010) and one down, approximately parallel to (110). Each Li tetrahedron forms two 5-membered and one 6-membered rings with (Si,Al) tetrahedra, which help to stabilize the lithium position according to Li and Peacor [46].

The solid solutions are isostructural with β-spodumene but their lattice parameters differ from those of the stoichiometric β-spodumene. The lattice parameters $a$ and $c$ increase with an increasing content in aluminum which is more voluminous [47, 32]. The β-spodumene solid solution of the glass-ceramic C, $Li_2O{\cdot}Al_2O_3{\cdot}7.5SiO_2$, is poorer in Al and Li than the stoichiometric β-spodumene and the unit cell is smaller than the pure β-spodumene one. Moreover, the unit cell contains only 2.5 Li atoms on average instead of 4 for the β-spodumene. Some pairs of 8-fold general position sites stay unoccupied. The number of available sites for the diffusion movements is therefore higher.

### 3.4.2. Structural study by infrared spectroscopy

More information about the materials fine structure can be obtained from infrared spectroscopy data.

Up to now, some infrared spectroscopy studies have been performed on glassy and crystallized materials of LAS system [48–53], but the band assignment, when it exists, is uncertain. The main spectral features and the differences between the three material spectra have been observed. However it should be noticed that, due to the complexity of the material composition, the interpretation of the infrared spectra is difficult.

As shown in Fig. 16, the spectrum can be divided in two spectral ranges: the first one extends from 4000 to 1500 $cm^{-1}$ and the second one from 1500 to 400 $cm^{-1}$.

The high frequency spectral range (4000 to 1500 $cm^{-1}$) is identical for the three materials; it exhibits the same features:

- a wide band ~3440 $cm^{-1}$ and a shoulder around 1630 $cm^{-1}$ which are characteristic of the presence of molecular water probably in the KBr pellets.
- two low intensity bands at 2920 $cm^{-1}$ and 2850 $cm^{-1}$ attributed to symmetric and asymmetric vibrations of -$CH_2$ group respectively. The presence of $CH_2$ is certainly due to impurities introduced during the pellets preparation.

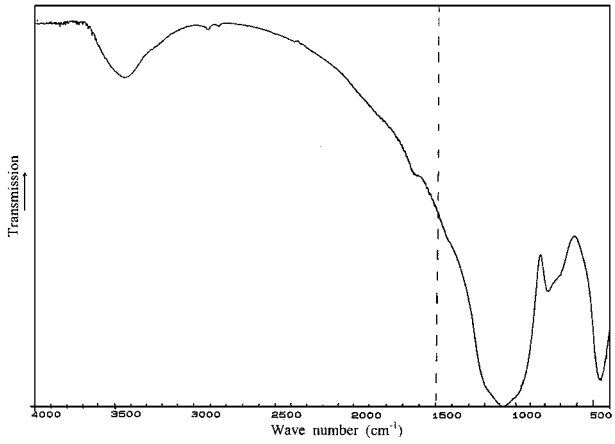


*Figure 16* FTIR spectrum of glass A with the high-frequency range (4000 $cm^{-1}$–1500 $cm^{-1}$) common to the three materials A, B and C.

– a weak band, located near 2350 $cm^{-1}$, which is associated with the asymmetric stretching vibration of $CO_2$. This is confirmed by Glaze *et al*. [54] and Adams [55] who attribute this band to atmospheric $CO_2$.

This frequency spectral range is not the most important spectrum range because it is not representative of the sample. Therefore, the attention must be focused on the low frequency range (1500 to 400 $cm^{-1}$) which is characteristic of the studied materials.

*3.4.2.1. Glass A.* The diffuse nature of the spectrum indicates that it is relative to a disordered structure (low-frequency range (1500–400 $cm^{-1}$) in Fig. 16). In this range, the FTIR spectrum is alike to the vitreous $SiO_2$ spectrum and depicts three main absorption bands (Fig. 16).

The wide band at high frequency (∼1080 $cm^{-1}$) is characteristic of asymmetric stretching vibrations of the Si-O-Si bonds, $\nu_{AS}$(Si-O-Si), in silicates with three-dimensional network structure or in vitreous $SiO_2$ [19, 56–58]. In LAS-type glasses used for commercial glass-ceramics, aluminum is preferably located in the tetrahedral network and acts as network former as silicon. Thus, it is likely that the asymmetric stretching vibrations of Si-O-Al bonds, $\nu_{AS}$(Si-O-Al), take part in this band, as it would be specified further.

The band around 460 $cm^{-1}$ is attributed to the O-Si-O bending vibration, $\delta$(O-Si-O). It is a characteristic band of the three-dimensional network silicate glasses and more generally of the tectosilicates; in the glassy silica, this band is located at 468 $cm^{-1}$ [57]. It can also be due to the symmetric stretching vibrations of $LiO_4$ tetrahedra and $MgO_6$ octahedra, which generally appear in this frequency range [59].

The weakest band between 800 and 700 $cm^{-1}$, corresponds to the symmetric stretching of Si-O-Si bond, $\nu_S$(Si-O-Si), which appears at the same frequency for the vitreous silica. This band shows a strong shoulder ∼725 $cm^{-1}$. An analogous phenomenon has been observed by Roy in his study on the $(xM_2O{-}xAl_2O_3{-}(1-2x)SiO_2)$ alkali aluminosilicate glasses [48], where the 800 $cm^{-1}$-band gradually separates in two bands with first the appearance of a shoulder (∼720 $cm^{-1}$) when $Al_2O_3$ increases. According to studies performed on aluminosilicate glasses, the band (∼730 $cm^{-1}$) has been assigned to the $\nu(Al^{IV}\text{-}O)$ vibrations [48, 49, 60]. Hence, in the FTIR spectrum, the shoulder (∼725 $cm^{-1}$) seems to reveal the existence of tetracoordinated Al. The splitting in two bands, which indicates the presence of two vibrational modes, is due to the fact that, in the tetrahedral vitreous network, the aluminum atoms create their own sites not equivalent to those of the silicon atoms [48]. The Al atoms form $AlO_4$ tetrahedra which insert into silicate three-dimensional network in forming Si-O-Al bonds. These bonds give rise to asymmetric $\nu_{AS}$(Si-O-Al) and symmetric $\nu_S$(Si-O-Al) vibrations, which are located close to those of Si-O-Si bonds. So, the wide band centered at 1080 $cm^{-1}$ is associated, as previously mentioned, to asymmetric $\nu_{AS}$(Si-O-(Si,Al)) valence vibrations and the one at 790 $cm^{-1}$ to their $\nu_S$(Si-O-(Si,Al)) symmetric vibrations.

There is no absorption band near 950 $cm^{-1}$ which suggests that there is no non-bridging oxygen ions in the glass A [60, 61]. This would confirm that Al atoms are tetracoordinated. If the Al atoms were acting as modifiers, they would be hexacoordinated $Al^{3+}$ ions, which would be characterized by the presence of a band around 550 $cm^{-1}$[50, 60, 62, 63] but this band does not appear in the glass A spectrum.

It seems therefore that the structural network of the glass A is composed of a former three-dimensional aluminosilicate network where the $SiO_4$ and $AlO_4$ tetrahedra are more or less uniformly distributed. The glass A does not contain non-bridging oxygen ions and the alkali and earth-alkali ions insert in the cavities and act as charge balancers compensating for the negative charge due to Si substitution by Al.

*3.4.2.2. Glass-ceramics B and C.* In the 1500–400 $cm^{-1}$ range, the infrared spectra relative to glass-ceramics B and C (Figs 17 and 18) show spectral change

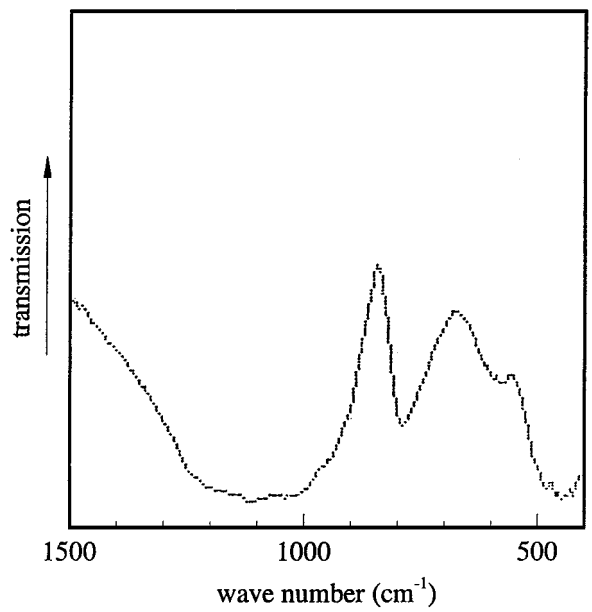


*Figure 17* Low-frequency infrared spectrum (1500 $cm^{-1}$–400 $cm^{-1}$) of glass-ceramic B.

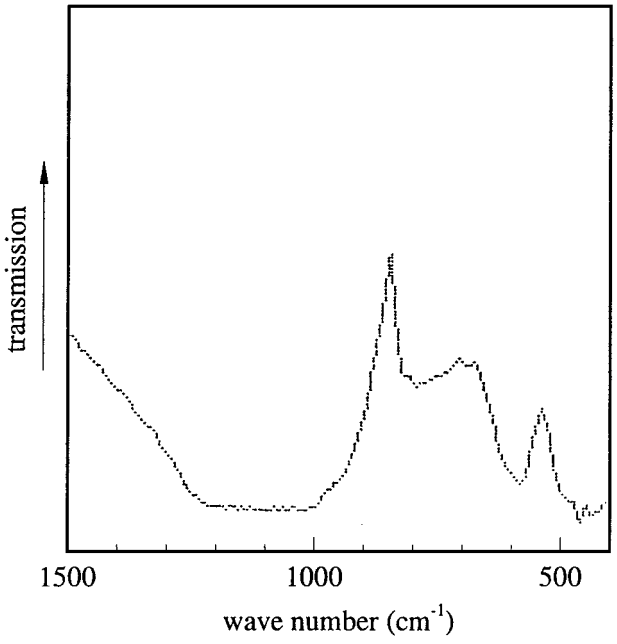


*Figure 18* Low-frequency infrared spectrum (1500 $cm^{-1}$–400 $cm^{-1}$) of glass-ceramic C.

in comparison to the glass A spectrum. The spectra are less diffuse, which confirms that materials B and C are partially crystallized. As for the glass A, these spectra show a wide intense band centered at 1080 $cm^{-1}$ and a band around 440 $cm^{-1}$.

The high frequency band, centered at 1080 $cm^{-1}$, is assigned to the stretching vibrations of Si-O-(Si,Al) bonds, which is characteristic of the tectosilicates. So, in the stuffed $\beta$-quartz solid solution of B as well as in the $\beta$-spodumene solid solution of C, which are isostructural with $\beta$-quartz and keatite respectively, Al substitutes partially for Si in tetracoordinated position in the three-dimensional crystalline network. It is likely that the residual vitreous aluminosilicate phase also contributes to this band. In spite of the pellet saturation, a slight shoulder is noticed near 950–960 $cm^{-1}$; this feature is linked with the $\nu$(Si-$O^-$) vibration mode [60, 61]. So it seems that there are non-bridging oxygen ions in the residual vitreous phase of the glass-ceramics B and C, whose composition is different from the composition of the glass A.

In both glass-ceramic spectra, the band ($\sim$440 $cm^{-1}$), which is the second main characteristic band of tetracoordinated Si and is assigned to $\delta$(O-Si-O), is observed. However, it is located at lower frequency than the band of glass A. This could be due to "the lattice vibration" which occurs at lower frequency. Other entities, such as $LiO_4$, may also contribute to this band.

The significant spectral modifications between the glass A and the glass-ceramics (B and C) appear in the intermediate frequency range, between 850 and 500 $cm^{-1}$. Contrary to the glass A spectrum, the spectra of the glass-ceramics depict two bands: one located at $\sim$770 $cm^{-1}$ and the other one at $\sim$570 $cm^{-1}$. For glass-ceramic B, the first one is well-defined and strong, and the second one is weak, whereas it is the opposite for the glass-ceramic C. As glass-ceramics B and C have the same chemical composition, it may let suppose that it is the same element which takes part in both bands but with a different coordination.

The band near 770 $cm^{-1}$ is probably due to $\nu_S$(Si-O-(Si,Al)) and $\nu$(Al-O) stretching vibrations [48, 50, 60]. The $\beta$-eucryptite and $\beta$-spodumene solid solutions are composed of a crystalline three-dimensional aluminosilicate framework where the Si and Al atom distribution is random. The $SiO_4$ and $AlO_4$ sites are so equivalent, which gives rise to a single absorption band. According to previous studies, this band exists in the spectra of the $\beta$-eucryptite [64, 65] and in the $\beta$-eucryptite/$\beta$-quartz solid solutions [52]; they also appear in the $\beta$-spodumene but however they are weaker [50, 63, 65].

The band around 570 $cm^{-1}$ could be assigned to the $MgO_4$ or $AlO_6$ vibrational groups, which generally show an absorption in this frequency range [59, 62]. In both glass-ceramics, Mg content is low ($\sim$1.7 mol%) and has 4-fold coordination. In glass-ceramic B, Mg is partially substituted for Li in the $\beta$-quartz solid solution and in glass-ceramic C, Mg is mainly located in the normal spinel phase.

For glass-ceramic B, the band at 770 $cm^{-1}$ is very intense, while the one located at 570 $cm^{-1}$ is very weak, which suggests that almost all the aluminum atoms are 4-fold coordinated and enter into the tetrahedral sites in the aluminosilicate network of the $\beta$-eucryptite/$\beta$-quartz solid solution $(MgO,ZnO,Li_2O)\cdot Al_2O_3\cdot nSiO_2$ with $n \sim 6$. However, it seems that there is a low amount of hexacoordinated Al, which are in the residual vitreous phase.

For glass-ceramic C, contrary to glass-ceramic B, the band at 570 $cm^{-1}$ is more intense and better defined than the band at 770 $cm^{-1}$. As the Mg contribution is the same for both glass-ceramics, the predominance of the band at 570 $cm^{-1}$ compared with the band at 770 $cm^{-1}$ in glass-ceramic C can not be ascribed to Mg. The high intensity of the band at 570 $cm^{-1}$ can thus be attributed to the $\nu(Al^{IV}$-O) vibration, and thus to the presence in high content of 6-fold coordinated Al. In glass-ceramic C, all the Al atoms do not therefore belong to the aluminosilicate network of the $\beta$-spodumene solid solution ($Li_2O\cdot Al_2O_3\cdot nSiO_2$ with $n \sim 7.5$) and a great part is in 6-fold coordination. Indeed, a part of Al is located in the secondary crystalline phases, namely spinel ($MgAl_2O_4$) and gahnite ($ZnAl_2O_4$) identified in Section 3.2.1. On the other hand, a non negligible Al amount may also exist in the residual vitreous phase, in which Al atoms would act as modifiers and would be present as $Al^{3+}$ ions in octahedral sites. This presence of 6-fold coordinated Al ($Al^{3+}$) in the vitreous residual phase would be in agreement with the presence of non-bridging oxygens, as previously mentioned.

The FTIR study confirms that the main crystalline phase of glass-ceramics B and C, the $\beta$-quartz solid solution and the $\beta$-spodumene solid solution respectively, are composed of a three dimensional network of $(Al,Si)O_4$ tetrahedra, where Al are randomly substituted for Si. Moreover, the FTIR analysis shows that, contrary to glass A, the residual vitreous phase of each glass-ceramic contains non-bridging oxygens. However, spectral differences exist between the two

glass-ceramics. In glass-ceramic B, almost all the Al atoms enter into the tetrahedral sites in the aluminosilicate network of the $\beta$-quartz solid solution and a low amount of hexacoordinated Al is present in the residual vitreous phase. On the contrary, in glass-ceramic C, all the Al atoms do not belong to the aluminosilicate network of the $\beta$-spodumene solid solution. Indeed, a great part of Al atoms is 6-fold coordinated and is located in the secondary phases (spinel and gahnite) and in the residual vitreous phase.

FTIR experiments have thus allowed to obtain structural information, notably on the atomic arrangement, such as the coordination of different elements (e.g. Al and non-bridging O), which the other methods could not give. They have also allowed to characterize more precisely the glass A and the residual vitreous phase of each glass-ceramic.

## 4. Conclusion

Two commercial LAS-type glass-ceramics (B and C) and their parent glass (A) have been extensively studied. Their microstructure has been characterized by several complementary techniques at different scales (SEM, DTA, XRD, TEM and FTIR).

The glass A is an aluminosilicate glass with a three-dimensional framework of $(Si,Al)O_4$ tetrahedra. The $Li^+$, $Mg^{2+}$ and $Zn^{2+}$ ions maintain the charge balance and this glass does not contain non-bridging oxygen.

This study has also shown that the glass-ceramics B and C, identified as "$\beta$-quartz" and "$\beta$-spodumene" glass-ceramics respectively, although they derive from the same parent glass, exhibit different microstructures.

The two glass-ceramics have a high crystallinity rate ($\sim$90%), but different grain size and distribution. The glass-ceramic B with a mean grain size of 50 to 100 nm is transparent while glass-ceramic C with a mean grain size of 1 $\mu$m is opaque. On the other hand, the residual intergranular vitreous is thinner and more uniformly distributed in the "$\beta$-quartz" glass-ceramic than in the "$\beta$-spodumene" glass-ceramic. However, in both cases, the residual glassy phase contains non-bridging oxygen ions.

The main crystalline phase of glass-ceramic B is an hexagonal stuffed $\beta$-quartz solid solution whose composition is $[Zn_{0.123}Mg_{0.173}Li_{1.408}]O{\cdot}Al_2O_3{\cdot}6SiO_2$, while the main crystalline of glass-ceramic C is a tetragonal $\beta$-spodumene solid solution with the following composition $Li_2O{\cdot}Al_2O_3{\cdot}7.5SiO_2$. In the stuffed $\beta$-quartz solid solution, the interstitial sites are pseudo-octahedral; the stuffing Li ions, which insert in these sites of the aluminosilicate framework to maintain the charge balance, form irregular $LiO_4$ tetrahedra. Zn and Mg atoms present in glass-ceramic B substitute for Li ions in the interstitial sites.

In the $\beta$-spodumene solid solution, the Li ions are located in paired 8-fold sites and form very distorted $LiO_4$ tetrahedra. Contrary to the glass-ceramic B, in glass-ceramic C, Mg and Zn are not in the main crystalline phase but form the secondary phases, spinel ($MgAl_2O_4$) and gahnite ($ZnAl_2O_4$), where there are tetracoordinated and Al is hexacoordinated.

Moreover, the nature of the secondary phases is also a difference between the two glass-ceramics. $TiZrO_4$ is present in both glass-ceramics but glass-ceramic C contains in addition gahnospinel $(Zn, Mg)Al_2O_4$ as secondary phase.

The different characterization techniques employed in this study have allowed to obtain complementary and detailed microstructural data on the complex LAS-type parent glass and both glass-ceramics. This extensive microstructural study has been essential for the understanding and interpretation of the mechanical relaxation mechanisms in these materials.


## Acknowledgements

The authors appreciate the generosity of Corning Europe Inc. (Corning S.A.) for providing the materials used in this study. Thanks are extended to Prof. J. H. Thomassin (HYDRASA, University of Poitiers, France) for his kind collaboration, as well as M. F. Abrioux and M. Garais for their technical assistance. The authors are grateful to H. Garem (LMP, University of Poitiers) for her help in the MET examinations.


## References


1. S. D. STOOKEY, US Patent 2 920 970, January (1960).
2. *Idem. Ind. Engng. Chem.* **51** (1959) 805.
3. R. A. EPPLER, *J. Amer. Ceram. Soc.* **46** (1963) 97.
4. G. H. BEALL, B. R. KARSTETTER and H. L. RITTLER, *ibid.* **50** (1967) 181.
5. A. NORDMANN and Y. B. BCHENG, *J. Mater. Sci.* **32** (I997) 83.
6. D. R. STEWART, "Advances in Nucleation and Crystallisation in Glasses" (Am. Ceram. Soc., 1971) p. 83.
7. M. J. BUERGER, *Am. Mineralogist* **39** (1954) 600.
8. S. RAY and G. M. MUCHOW, *J. Amer. Ceram. Soc.* **51** (1968) 678.
9. G. H. BEALL and D. A. DUKE, *J. Mater. Sci.* **4** (1969) 340.
10. G. PARTRIDGE, *Glass Technology* **23** (1982) 133.
11. C. T. LI, *Z. Kristallogr.* **132** (1970) 118.
12. M. D. KARKHANAVALA and F. A. HUMMEL, *J. Amer. Ceram. Soc.* **36** (1953) 393.
13. T. I. PROKOPOWICZ and F. A. HUMMEL, *ibid.* **39** (1956) 266.
14. G. H. BEALL, B. R. KARSTETTER and H. L. RITTLER, *ibid.* **50** (1967) 181.
15. G. PETZOLDT, *J. Glastechn. Ber.* **40** (1967) 385.
16. L. ARNAULT, A. RIVIERE and B. LUCAS, *J. Non-Cryst. Solids* **210** (1997) 87.
17. L. ARNAULT, PhD thesis, Université de Poitiers, France, 1997.
18. D. G. GROSSMAN, in "Concise encyclopedia of Advanced Ceramic Materials," edited by R. J. Brook (Pergamon Press, 1991) p. 170.
19. J. ZARZYCKI, in "Les verres et l'tat vitreux" (Masson, 1982).
20. A. RAMOS, PhD thesis, Université de Paris VI, 1988.
21. P. E. DOHERTY, D. W. LEE and R. S. DAVIS, *J. Amer. Ceram. Soc.* **50** (1967) 77.
22. H. S. KIM, R. D. RAWLINGS and P. S. ROGERS, *Br. Ceram. Trans. J.* **88** (1989) 21.
23. M. A. SUBRAMANIAN, D. R. CORBIN and R. D. FARLEE, *Mat. Res. Bull.* **21** (1986) 1525.
24. C. T. LI, *Acta Cryst.* **B27** (1971) 1132.
25. *Idem., Z. Kristallogr.* **132** (1970) 118.
26. M. IWATSUKI and T. FUKASAWA, *Nihon Kagakukai-shi* **10** (1976) 1569.
27. M. IWATSUKI, M. TANAKA and T. FUKASAWA, *ibid.* **3** (1974) 505.

28. M. IWATSUKI, N. TSUKADA and T. FUKASAWA, *Bull. Chem. Soc. Japan* **48** (1975) 1217.
29. R. ROY, *Z. Kristallogr*. **111** (1959) 185.
30. V. MAIER and G. MÜLLER, *J. Amer. Ceram. Soc.* **70** (1987) 176.
31. K. NAKAGAWA and T. IZUMITANI, *J. Non-Cryst. Solids* **7** (1972) 168.
32. B. J. SKINNER and H. T EVANS, *Am. J. Sci., Bradley Vol*. **258A** (1960) 312.
33. W. OSTERTAG, G. R. FISCHER and J. P. WILLIAMS, *J. Amer. Ceram. Soc*. **51** (1987) 651.
34. T. FUKASAWA, M. IWATSUKI and K. YAMAGUCHI, *Bunseki Kagaku* **22** (1973) 745.
35. W. A. DEER, R. A. HOWIE and J. ZUSSMAN, "An introduction to the rock-forming minerals" (Longman, 1983).
36. I. M. TERESHCHENKO, N. M. BOBKOVA, G. E. RACHKOVSKAYA and L. G. DASHCHINSKIJ, *Fiz. Khim. Stekla* **7** (1981) 570.
37. R. A. FEDOROVA, E. V. SOBOLEV and V. V. KRAVCHENKO, *Steklo i keramika* **11** (1991) 7.
38. C. T. LI, *Acta Cryst.* **B27** (1971) 1132.
39. M. C WANG and M. H. HON, *Ceramics International* **19** (1993) 223.
40. M. H. LEWIS, J. METCALF-JOHANSEN and P. S. BELL, *J. Amer. Ceram. Soc*. **62** (1979) 278.
41. T. I. BARRY, D. J. CLINTON and L. A. LAY, "Ceramic Microstructures 76" (Westview Press, Boulder, 1976) p. 479.
42. W. SCHREYER and J. F. SCHAIRER, *Z. Kristallogr*. **116** (1961) 60.
43. C. T. LI, *ibid.* **127** (1968) 327.
44. C. T. LI and P. J. SHLICHTA, *ibid.* **140** (1974) 100.
45. J. SHROPSHIRE, P. P. KEAT and P. A. VAUGHAN, *ibid.* **112** (1959) 409.
46. C. T. LI and D. R. PEACOR, *ibid.* **126** (1968) 46.
47. A. ZIADI, J. P. MERCURIO and B. FRIT, *Mat. Res. Bull*. **19** (1984) 1015.
48. B. N. ROY, *J. Amer. Ceram. Soc.* **70** (1987) 183.
49. O. P. GIRIN, "The Structure of Glass" Vol. 3 (Consultants Bureau, New York, 1964) p. 105.
50. A. KOLESOVA, *Optics and Spectroscopy* **6** (1959) 20.
51. M. L. WANG, R. STEVENS and P. KNOTT, *Glass Technology* **23** (1982) 139.
52. *Idem., ibid.* **23** (1982) 238.
53. Y. N. KONDRAT'EV, *Opt. Spektry*. **18** (1965) 603.
54. F. W GLAZE, *Bull. Amer. Ceram. Soc*. **34** (1955) 291.
55. R. V. ADAMS, *Physics and Chemistry of Glasses* **2** (1961) 39.
56. H. H. MOENKE, "The Infrared Spectra of Minerals" edited by V. C. FARMER (Mineralogical Society, Monograph 4, 1974) p. 365.
57. R. J. P. LYON, *Nature* **196** (1962) 266.
58. S. PARKE, "The Infrared Spectra of Minerals" edited by V. C. FARMER (Mineralogical Society, Monograph 4, 1974) p. 483.
59. P. TARTE, "Physics of Non-Crystalline Solids" (Wiley, New-York, 1964) p. 549.
60. C. GARNIER, PhD thesis, Université de Rennes I, France 1994.
61. R. HANNA and G. J. SU, *J. Amer. Ceram. Soc*. **47** (1964) 597.
62. V. A. KOLESOVA, *Inorganic Materials* **1** (1965) 408.
63. L. A. IGNAT'EVA, *Optics and Spectroscopy* **6** (1959) 527.
64. V. A. KOLESOVA, *Izv. Akad. Nauk. SSSR* **1** (1963) 187.
65. V. A. FLORINSKAYA, E. V. PODUSHKO, I. N. GONEK and E. F. CHERNEVA, "The Structure of Glass" Vol. 3 (Consultants Bureau, New York, 1964) p. 96.

*Received 19 February 1998*
*and accepted 22 October 1999*